

Leigh A. Mrotek · C.C.A.M. Gielen · Martha Flanders

Manual tracking in three dimensions

Received: 15 March 2005 / Accepted: 11 October 2005 / Published online: 25 November 2005
© Springer-Verlag 2005

Abstract Little is known about the manual tracking of targets that move in three dimensions. In the present study, human subjects followed, with the tip of a hand-held pen, a virtual target moving four times (period 5 s) around a novel, unseen path. Two basic types of target paths were used: a peanut-shaped Cassini ellipse and a quasi-spherical shape where four connected semicircles lay in orthogonal planes. The quasi-spherical shape was presented in three different sizes, and the Cassini shape was varied in spatial orientation and by folding it along one of the three bend axes. During the first cycle of Cassini shapes, the hand lagged behind the target by about 150 ms on average, which decreased to 100 ms during the last three cycles. Tracking performance gradually improved during the first 3 s of the first cycle and then stabilized. Tracking was especially good during the smooth, planar sections of the shapes, and time lag was significantly shorter when the tracking of a low-frequency component was compared to performance at a higher frequency (−88 ms at 0.2 Hz vs. −101 ms at 0.6 Hz). Even after the appropriate adjustment of the virtual target path to a virtual shape tracing condition, tracking in depth was poor compared to tracking in the frontal plane, resulting in a flattening of the hand path. In contrast to previous studies where target trajectories were linear or sinusoidal, these complex trajectories may have involved estimation of the overall shape, as well as prediction of target velocity.

Keywords Smooth pursuit · Anticipatory response · Prediction · Hand tracking · Arm movement · Two-thirds power law

Introduction

Early studies of hand and eye tracking hinted at various reactive, predictive and anticipatory mechanisms (Poulton 1974; Yasui and Young 1975). More recent experiments show that during hand or eye tracking in one dimension, subjects require only a few trials to begin to anticipate the speed or frequency of a target repeatedly moving at the same constant speed or oscillation frequency (Barnes and Marsden 2002; Barnes et al. 2000); this phenomenon may be related to the well-known ability of humans to follow low-frequency, sinusoidal target motion with no time lag (Dallos and Jones 1963). Well-trained monkeys can also follow, with the eyes, more complex, two-dimensional (2D) target motions, and they do this with zero lag for low frequencies and lags gradually approaching 100 ms for higher frequencies (Kettner et al. 1996). However, in spite of these and other similar observations, the possible types and mechanisms of anticipation and prediction remain unclear, especially for targets that travel along complex trajectories in three dimensions.

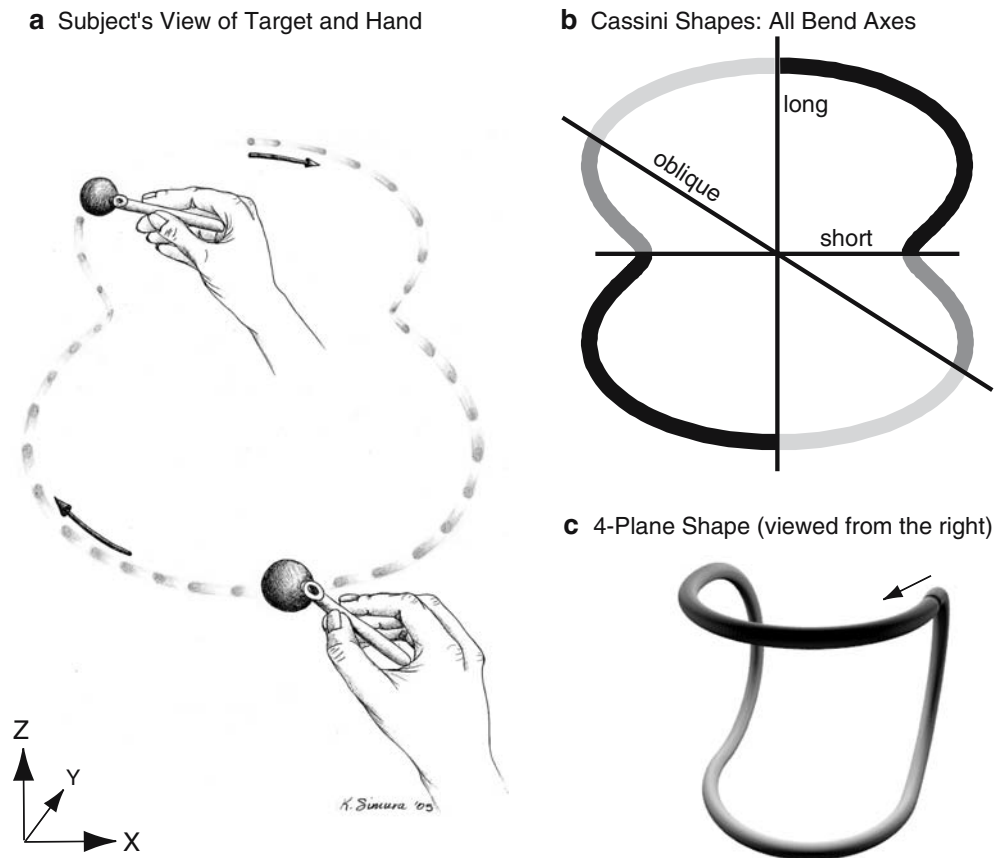
When subjects move the hand in two or three dimensions, they tend to follow several “rules” including: (1) use of small speed pulses for error corrections, (2) piecewise planar hand paths due to maintenance of a particular phase relation between elbow and shoulder angles and (3) a lawful relation between hand speed and hand path curvature (Roitman et al. 2004; Soechting and Terzuolo 1986, 1987b; Viviani et al. 1987). These rules may also be followed during the tracking of complex target trajectories, and these characteristics may change over the course of several repetitions, as the shape and timing of the target path and trajectory become familiar.

Little work has been done on manual tracking in three dimensions (3D), but there are several reasons to

L. A. Mrotek · M. Flanders (✉)
Department of Neuroscience, University of Minnesota, 6-145
Jackson Hall, 312 Church St. S.E., Minneapolis, MN 55455, USA
E-mail: fland001@umn.edu
Tel.: +1-612-6246601
Fax: +1-612-6265009

C.C.A.M. Gielen
Department of Medical Physics and Biophysics,
Radboud University Nijmegen, Nijmegen, Netherlands

Fig. 1 The experiment was designed to allow subjects to gradually become familiar with novel, but symmetrical target trajectories. **a** The illustration shows how the pen tip followed the virtual target sphere around the unseen path of a Cassini shape (*dashed lines and arrows*). A schematic of the Cassini shape shows the axes along which bends occurred (**b**). The boundaries of the six sections are defined by each possible bend location. One 4-Plane shape is also shown (**c**). This shape was made by joining the ends of four semicircles. For clarity, this shape is shown rotated from the subject's perspective (20° around the vertical axis and 30° around the horizontal axis)



hypothesize that tracking performance in depth is relatively poor. Oculomotor tracking of targets in 3D is much better for azimuth and elevation, than for depth (vergence) (Gielen et al. 2004). Since gaze affects the accuracy of pointing (Bock 1986; Henriques et al. 1998; Medendorp and Crawford 2002), errors in ocular tracking may affect the accuracy of hand tracking (see also Soechting et al. 2001). Furthermore, errors for pointing to remembered targets in three dimensions are greater for the depth dimension than for the other two dimensions (Adamovich et al. 1998; Soechting and Flanders 1989a, b; Admiraal et al. 2003), and there are many potential strategies for tracking targets that move in depth (see, e.g., Harris and Drga 2005).

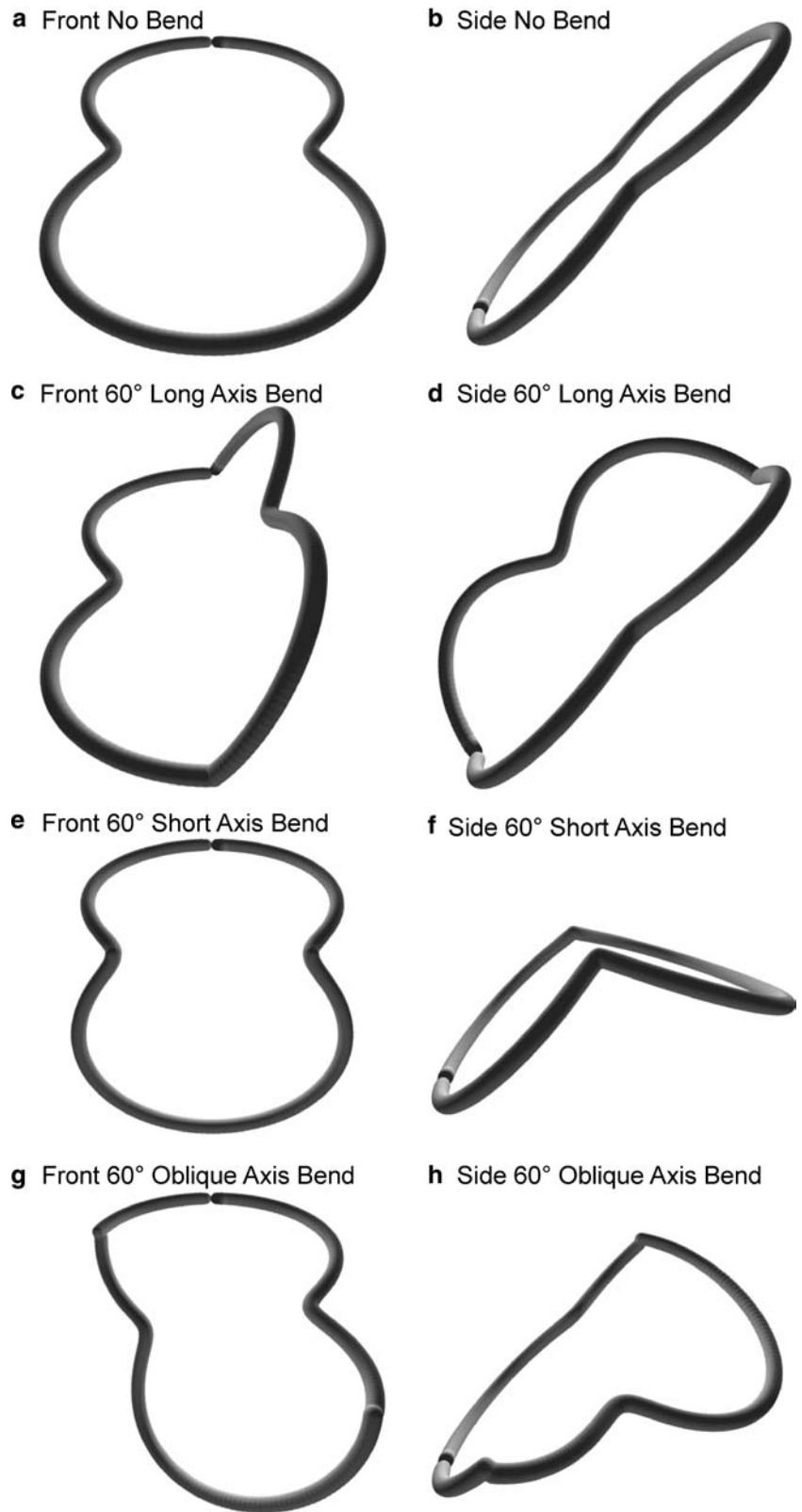
In the present study, we examined three aspects of manual tracking performance. First, we determined whether or not subjects gradually improved their performance while tracking a target that moved with a natural speed profile, four times in succession, along the invisible perimeter of a 3D shape. The shape was designed to be novel but symmetrical and piecewise planar. Secondly, we compared the more pulsatile response to an abrupt change in the plane of target motion to tracking performance during smoothly curved, planar sections. We expected that the first two aspects of our study would provide a quantification of

the process of target trajectory learning and prediction. The final aspect of our study was a comparison of hand tracking performance across the three dimensions of the target motion, i.e., we compared tracking in depth to tracking in the horizontal and vertical dimensions. A relatively poor performance in depth might correspond to a relatively poor use of visual cues for motion in depth.

Methods

The results of our experiment will be reported in a set of two papers: this paper and a companion paper (Flanders et al. 2005). In each recording session, a human subject first tracked (with the tip of a hand-held pen) a target that moved along the perimeter of a 3D shape (“tracking condition”). The target was a sphere (with a diameter of 2.5 cm) that moved along an unseen path, and the hand never blocked the view of the target (Fig. 1a). The subject then traced the same target path, now fully visible as a curved tube with the same diameter (Figs. 1c, 2; “tracing condition”). Finally, the subject drew the shape, in the same spatial location, from memory (“drawing condition”). This paper examines the manual tracking performance in the tracking condition, whereas the second paper (Flanders

Fig. 2 The main shape used in this experiment was a peanut-shaped Cassini ellipse (**a**). It was in a plane rotated 45° about the horizontal (X) axis, such that the bottom of the shape was closer to the subject. To generate another orientation (**b**) we rotated the shape 80° about the vertical (Y) axis, so that subjects saw a side view. In addition to these shapes, we altered the Cassini ellipse by folding it along three axes. It was bent along the long axis (**c** and **d**), the short axis (**e** and **f**) and an oblique axis (**g** and **h**). In this figure, the magnitude of all the bends is 60° , but we also bent each shape 30° . For all conditions, the subject began at the location of the discontinuity and moved clockwise around the shape. All the shapes are shown from the perspective of the subject



et al. 2005) compares several other aspects of the arm movements (e.g., planarity and speed/curvature relations) across all three conditions (tracking, tracing and drawing). The relative locations of the body, arm and

target are shown in Fig. 1 of the companion paper (Flanders et al. 2005). Subjects wore red/green glasses (as described below) and eye movements were not recorded.

Table 1 Shape properties

Cassini ellipse shapes	
Orientations	Front, side
Bend locations	Long axis, short axis, oblique axis
Bend magnitude	30°, 60°
4-Plane shapes	
Size	Small, medium, large

Seventeen different shapes were presented. Cassini shapes were presented in front and side views. Each of the Cassini shapes could have no bend or could be bent along a long, short or oblique axis by 30° or 60°. The 4-Plane shape was presented in small, medium and large sizes

Target shapes

Our aim was to create shapes that would be somewhat unfamiliar to subjects. We used two basic types of target path: a peanut-shaped Cassini ellipse (“Cassini shape,” Figs. 1b, 2) and a more spherical shape where four connected semicircles lay in horizontal and vertical planes (“4-Plane shape,” Fig. 1c). The Cassini shapes were modified by showing them from front and side orientations, and they were also folded along one of the three axes (Table 1). The 4-Plane shapes were shown in three different sizes (Table 1).

Cassini ellipse shapes

Eight of the 14 Cassini shapes are shown in Fig. 2. All of the shapes are rendered from the subject’s perspective; the subject’s eyes were aligned with the center of the shape. The shapes were composed of planar curved segments, and to make the target motion as natural as possible, within each plane we programmed the target speed to approximately obey the two-thirds power law (Lacquaniti et al. 1983). Thus, speed changed throughout the Cassini shapes, but the average speed was 26 cm/s.

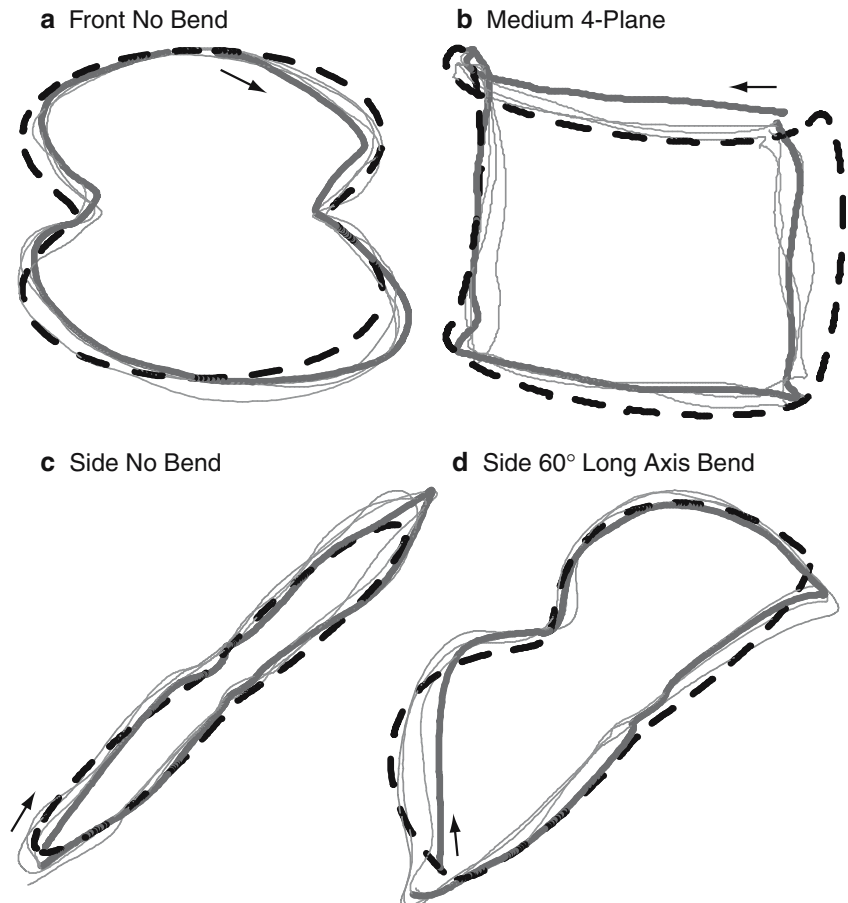
In Fig. 2a, b, we show the basic shape without bends, in frontal and side orientations, respectively. When viewed from the subject’s perspective or from above, the target always traveled clockwise around the unseen path. The word “indent” will be used to refer to the impressions between the two main lobes of the shape; they occurred at times 1,250 and 3,750 ms in each 5,000 ms cycle. The equations used to make the basic (Front No Bend) Cassini shape were:

$$X_{i=1:300} = R(1 + A \cos(2i)) \cos(i), \quad (1)$$

$$Z_{i=1:300} = 1.5R(1 + A \cos(2i)) \sin(i), \quad (2)$$

where $R=32$ cm and $A=0.5$. We used a right-handed coordinate system with the Z-axis in the vertical direction, the X-axis in the frontal plane, horizontal direction,

Fig. 3 Hand paths approximated the unseen target path quite well. The target path for four shapes is shown with a *thick dashed line*: Front No Bend shape (a), Medium 4-Plane shape (b), Side No Bend shape (c), Side 60° Long Axis Bend shape (d). One subject’s tracking performance is also shown. The data from the first cycle are graphed as a *thick line* and cycles 2–4 are graphed as *thin lines*. Arrows denote the starting point and the direction



and the *Y*-axis in depth (inset, Fig. 1a). The width of the shape was 32 cm and the long axis was 48 cm.

To give them depth, the Cassini shapes were then rotated 45° around the horizontal axis through the center of the shape. For the frontal orientation (Fig. 2a), the bottom of the shape was closer to the subject (thus the bottom appears larger in the 3D rendering). For the side orientation (Fig. 2b), the shape was also rotated 80° around the vertical axis. Another difference between the front and side orientations was that the starting position was at the top for the front orientation and at the bottom for the side orientation. In Fig. 2, starting position is depicted as a discontinuity.

Figure 1b and Table 1 list the axes along which the Cassini shapes were folded. The word “bend” will be used to refer to a perimeter location where the shape was folded. The bends were either 30° or 60° (see Table 1), but only the 60° bends are shown in Fig. 2. Figure 2c, d shows the shape bent along the long axis for the frontal and side orientations, respectively. Figure 2e, f shows the shape bent along the short axis, and Fig. 2g, h shows the shape bent along the oblique axis.

4-Plane shapes

The 4-Plane shapes were made from four semicircles, each placed in a plane perpendicular to the plane of the previous semicircle (Fig. 1c). Two semicircles were in horizontal planes and the openings faced away from the subjects; two were in parasagittal planes and the openings faced towards the subject. Each semicircle for the small 4-Plane shape had a radius of 8 cm; therefore the shape was 16 cm in the frontal plane and 16 cm in depth. The medium 4-Plane shape had radii of 14 cm, and the large 4-Plane shape had radii of 20 cm. For the small shape, the target moved at a constant speed of 11.42 cm/s, for the medium shape at 19.99 cm/s and for the large shape at 28.56 cm/s.

Procedures

All experimental procedures were in accordance with the human subjects regulations of Radboud University Nijmegen, where the recording sessions took place. Six subjects volunteered for the experiment (four females and two males; four right handed and two left handed; average age 33 ± 12 (SD) years). Two subjects (one right and one left handed) repeated the experiment and for these subjects, corresponding data (such as error or lag) from the two sessions were averaged. Subjects were presented with the shapes in a pseudorandom order; each of the 17 shapes was presented once (i.e., seven Cassini shapes in frontal view, seven Cassini shapes in side view and three 4-Plane shapes). For every shape, subjects were first asked to track a single moving target, and then after short rests of about 30 s, they traced and then drew from memory. For the tracking trials, the

target continued to move around the shape four times. Each complete revolution around the shape will be termed a “cycle.”

Measurement system

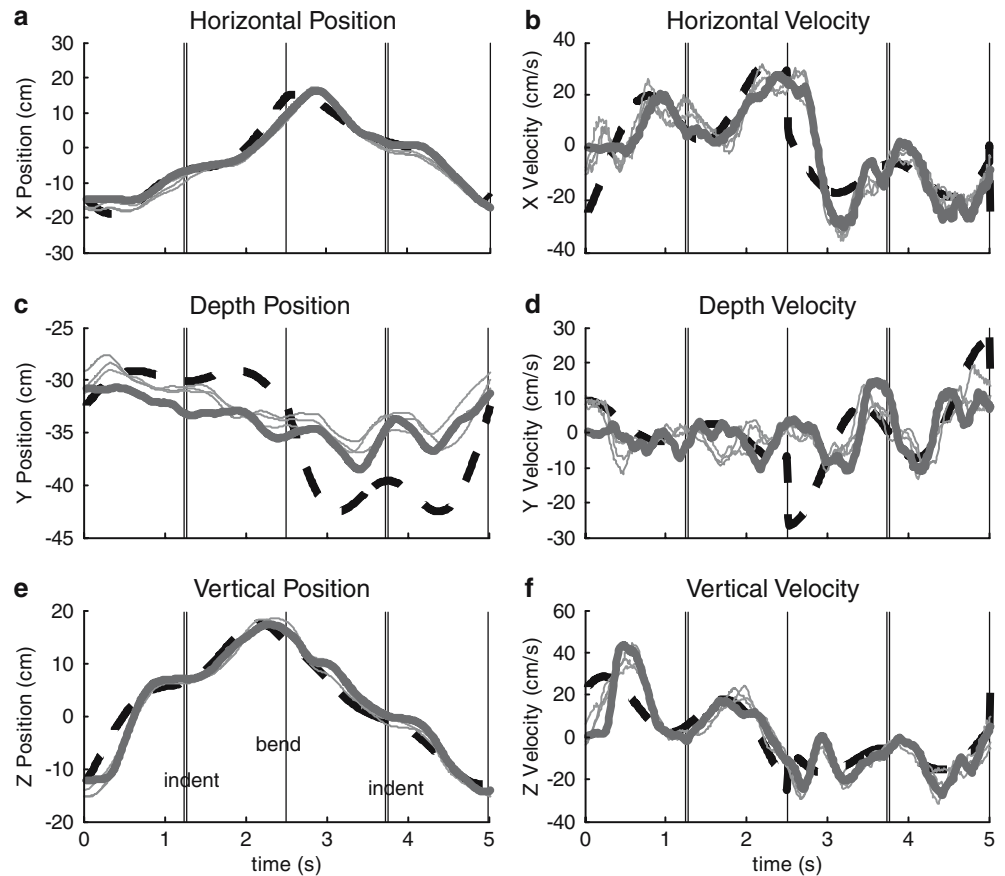
Infrared light-emitting diode markers were placed on the right shoulder, elbow and wrist and on the tip of a pen-like object held in the right hand. The pen tip extended 2 cm from the tip of the index finger (see Fig. 1a). Subjects were asked to track, trace or draw with the tip of the pen and were required to refrain from bending the wrist. The 3D locations of the markers were recorded with an Optotrak 3020 system (Northern Digital Inc.) at 100 Hz and with a precision of better than 0.15 mm in all dimensions. The Optotrak system was mounted from the ceiling above the subject at a distance of approximately 2.5 m from the subject, tilted down at an angle of 30° relative to the ceiling. For the analyses presented in this paper, we only examined the movement of the marker on the pen tip (the “hand” marker).

Target projection system

Targets were produced using a 3D virtual reality system. The room lights were dimmed as the subject donned red/green glasses and sat with the head at a distance of 90 cm from a large vertical screen (2 m × 2 m). Two images of a ball in front of a checkerboard pattern background were rear-projected onto the screen, one in green representing the projection of the 3D scene as viewed by the left eye and one in red representing the projection of the 3D scene as viewed by the right eye, using an LCD projector (Philips 4750) with a frame rate of 60 Hz. Custom software was used to calculate the desired locations and sizes of the projection of the checkerboard pattern and the ball on the projection screen providing the subject with stereovision when viewed through the red (Kodak Wratten no. 25) and green (Kodak Wratten no. 58) glasses, for the right and left eyes, respectively. The images for the left and right eyes were generated in the proper perspective relative to the observer such that the ball was perceived in front of the checkerboard pattern, relative to the subject. The position of the ball could change relative to the checkerboard pattern, which was always at the same position. Due to strong disparity and size cues, this binocular presentation gave the impression of a bright sphere moving through space in front of a dimmer checkerboard background.

The virtual reality system was initially calibrated by presenting a small virtual reality sphere with a diameter of 1 cm at various positions in space relative to a subject. The virtual targets were presented for 2 s and then disappeared. Subjects were instructed to bring the tip of the index finger to the perceived target position as soon as the target disappeared. These pointing positions were

Fig. 4 Tracking performance differed across dimensions and target parameters. Patterns of target and hand motion are shown for one subject, for the Side 60° Long Axis Bend shape. This is the same trial as presented in Fig. 3d. In each graph, the data from the first cycle are graphed as a *thick line* and cycles 2–4 are graphed as *thin lines*. The target motion is graphed with *thick dashed black lines*. Vertical double lines indicate times when the target was at an indent of the shape. The vertical single lines (including times 0 and 5,000 ms) indicate times when this shape had an abrupt bend. The top, left panel shows the frontal plane, horizontal position (a); the middle, left panel shows the position in depth (c); and the bottom, left panel shows the vertical position (e). The top, right panel shows the horizontal velocity (b); the middle, right panel shows the velocity in depth (d); and the bottom, right panel shows the vertical velocity (f)



compared to the position of the fingertip when subjects were instructed to point to the position of real targets at the same positions in 3D space as the programmed virtual reality targets. Mean errors between pointing positions to the virtual and real targets were less than 4% for targets in the frontal plane and less than 7% for the depth dimension.

For a proper perspective of the 3D virtual target relative to the subject, the inter-pupillary distance has to be taken into account in the software for the 3D virtual projection of the stimuli. For this experiment, all target trajectories were generated assuming that the inter-pupillary distance was 6 cm for each subject. This created small differences between the programmed target position and the perceived target position. To correct for these subject-specific differences in inter-pupillary distance, use of depth cues and strategies for placement of the pen tip relative to the target, during the data analysis, we calibrated the target trajectories based on each individual subject's performance during the tracing condition (i.e., when the pen tip was moved around the fully visible shapes). First, we used regression analysis to find the best parameters to center and scale the intended target path to the subject's tracing path for each shape individually. Then, we combined the calculated regression parameters to scale all of the target paths for each subject according to a single linear 3D gain and bias. The calibrated target paths then used in the analysis

were similar to the programmed target paths. For example, the target shapes shown in Fig. 3 (thick dashed lines) are the result of the calibration procedure.

Data analysis

Cycles and sections

For each shape, the target moved in four consecutive cycles. For the Cassini shapes, each target cycle lasted 5 s; for the 4-Plane shapes, each target cycle lasted 6.7 s. During analysis, each cycle of each Cassini shape was separated into subcycles, which were defined by the six possible bends and indents (see Fig. 1b).

Position and velocity

Data were collected in a 3D coordinate system and saved for offline analysis. As mentioned above, the right-handed coordinate system was defined such that the frontal, horizontal dimension was the *X*-axis (positive to the right of the subject), the depth dimension was the *Y*-axis (positive forward from the subject) and the vertical dimension was the *Z*-axis (positive upward).

The position of the target and hand was graphed over time for each dimension. For example, Fig. 4 (left

column, thick dashed line) shows the X -, Y - and Z -coordinates of the target trajectory for one Cassini shape (Side 60° Long). Note the magnified scale for the Y (depth) dimension in Fig. 4c. The position data were differentiated to compute velocity. The velocity over time for the Side 60° Long shape is depicted in the right column of Fig. 4 (thick, dashed line).

In each panel in Fig. 4, there are four vertical lines. As indicated in Fig. 4e, the double vertical lines denote the times of the midpoint of each indent (1,250 and 3,750 ms) and the single vertical lines denote the times when an abrupt bend occurred. For the Side 60° Long shape, the bends were located at the middle of the shape (2,500 ms) and at the end of each cycle (0 and 5,000 ms).

Direction

The direction of the target and hand motion was calculated in the frontal and the sagittal planes using the velocity from the dimensions that make up each plane:

$$\Theta_{\text{FP}} = \tan^{-1} \frac{V_z}{V_x}; \quad (3)$$

$$\Theta_{\text{SP}} = \tan^{-1} \frac{V_z}{V_y}. \quad (4)$$

Θ_{FP} and Θ_{SP} represent the directions in the frontal plane and the sagittal plane, respectively (see Fig. 5 for an example).

Distance, speed and direction error

For each point in time we calculated the distance between the 3D target and hand positions (distance error, E_{dis}):

$$E_{\text{dis}}(t) = \sqrt{(P_{\text{XT}}(t) - P_{\text{XH}}(t))^2 + (P_{\text{YT}}(t) - P_{\text{YH}}(t))^2 + (P_{\text{ZT}}(t) - P_{\text{ZH}}(t))^2}. \quad (5)$$

The subscript T indicates target position and the subscript H indicates hand position.

We used two methods to calculate the difference between the target and hand speed. First we found the signed speed error ($E_{\pm\text{spd}}$) by subtracting the hand speed from the target speed:

$$E_{\pm\text{spd}}(t) = \sqrt{(V_{\text{XT}}(t))^2 + (V_{\text{YT}}(t))^2 + (V_{\text{ZT}}(t))^2} - \sqrt{(V_{\text{XH}}(t))^2 + (V_{\text{YH}}(t))^2 + (V_{\text{ZH}}(t))^2}. \quad (6)$$

We also computed the magnitude of the velocity error or the unsigned speed error (E_{spd}) in a manner similar to the calculation of the distance error:

$$E_{\text{spd}}(t) = \sqrt{(V_{\text{XT}}(t) - V_{\text{XH}}(t))^2 + (V_{\text{YT}}(t) - V_{\text{YH}}(t))^2 + (V_{\text{ZT}}(t) - V_{\text{ZH}}(t))^2}. \quad (7)$$

We calculated the direction error in the two planes by finding the absolute difference between the target and hand directions:

$$E_{\text{dir}} = |\text{Dir}_T - \text{Dir}_H|. \quad (8)$$

The direction error was calculated in the frontal and sagittal planes separately.

Position, velocity and direction lag/lead

We tested whether the subjects were responding to the target motion or anticipating it by calculating a lag/lead measure for position, velocity and direction. Lag is given a negative value and lead is given a positive value. Cross-correlation analysis was used to find the overall time lag/lead for each cycle. All times from -350 to $+350$ ms were tested in 10 ms intervals to determine the lag and the correlation coefficient. A similar analysis was also applied to selected subsections of the data. In order to test for differences between various correlation coefficients, we converted them to Z -scores.

A full cycle was excluded from statistical analysis if the cross-correlation analysis did not reveal a peak within the ± 350 ms time interval (i.e., if the maximum value occurred at the maximum shift). Data representing the depth dimension or the sagittal plane had many more cycles excluded than did data representing the horizontal or vertical dimensions or the frontal plane. Of the 408 total cycles, those excluded were: 79 for depth position lag, 0 for horizontal position lag, 1 for vertical position lag, 29 for depth velocity lag, 1 for horizontal velocity lag and 1 for vertical velocity lag. The sagittal plane direction lag had 12 cycles excluded, whereas the frontal plane direction lag had only 1 cycle excluded.

We also quantified the transfer function of the hand motion (output) and target motion (input) at various frequencies by computing Bode plots. For this analysis, we applied the transfer function subroutine in LabVIEW

software (National Instruments, Inc.) to the data from four consecutive cycles. Because the frequency spectrum of the target motion was limited, we focused on the target's fundamental frequency (0.2 Hz) and the third harmonic (0.6 Hz). We then converted phase lag to time lag.

Instantaneous lag (in position)

In addition to using cross-correlation and frequency domain analyses to find the overall lag for the entire cycle, we also wanted to find the lag for each hand position, within each cycle (see Fig. 8). To do this, for each

instantaneous hand position, we calculated the distance to a range of possible positions of the target. We included all target positions from 1 s before the current

time until the current time. Thus, we generated a vector of distance error values:

$$\text{Error}_i(t) = \sqrt{(X_{H(t)} - X_{T(i)})^2 + (Y_{H(t)} - Y_{T(i)})^2 + (Z_{H(t)} - Z_{T(i)})^2}, \quad (9)$$

where the index i is the sample interval, which ranges from the current time at this hand position (t) to the time 1,000 ms earlier ($t-1,000$ ms). Thus, the subscript $H(t)$ indicates the hand position at the current time and the subscript $T(i)$ indicates all of the target positions from the current time to 1 s earlier. The result of Eq. 9 was a vector of error values for each hand position. We then searched for the minimum $\text{Error}_i(t)$ value and found the time difference between the time when the target was the closest ($\text{Time}(\min(\text{Error}_i(t)))$) and the current time t :

$$\text{Lag} = \text{Time}(\min(\text{Error}_i(t))) - t. \quad (10)$$

This time difference will be called the instantaneous lag (Lag). For comparison, we repeated this analysis to also allow for leads of up to 100 ms.

Results

Tracking position in three dimensions

The path of the hand marker (i.e., the LED on the pen tip) approximated the calibrated target path. Figure 3 displays position data for four shapes, tracked by one subject. The thick dashed lines represent the path of the target, the thick solid line shows the hand tracking for the first cycle and the thinner lines represent the second, third and fourth cycles. The first cycle had greater error. For example, in Fig. 3a the thick line starts out (arrow) farther away from the target line. This is also seen for the top semicircle in the Medium 4-Plane shape (Fig. 3b) and the first quarter of the Side 60° Long shape (Fig. 3d). The tracking for the next three cycles was fairly consistent. Across all conditions and all subjects, the tracking also appeared to be better in the frontal plane than in depth.

In the left column of Fig. 4, we show, for each dimension, the position of target and hand motion for one subject, for the Side 60° Long shape. The results displayed here are typical of all subjects. The dashed line represents the target motion, the thick solid line represents the hand motion during the first cycle and the thinner lines represent the hand motion for the remaining cycles. As explained under [Methods](#), the vertical double lines represent the times when the target was at the center of an indent and the single vertical lines represent the times when an abrupt bend occurred.

The subject was very accurate in tracking the target in the frontal plane, in both the horizontal and vertical dimensions (Fig. 4a, e). There was little position error, and the subject was fairly consistent across cycles. For the vertical dimension, the most error appeared to occur in the first 500 ms of each cycle, when the target was

traveling mostly upward (Fig. 4e). For the horizontal dimension, the most error occurred at the middle of each

cycle; this is when the target motion had an abrupt bend and reversed horizontal direction (2,500 ms; Fig. 4a). The subject also typically lagged behind the target, as evidenced by the hand data being shifted to the right relative to the target data.

The target position was not tracked as well in depth, and thus there were large depth position errors across the entire shape. For example, in Fig. 4c, the hand data show little modulation. During tracking, subjects typically made the tracked shapes flatter than their own traced shapes (which were used to scale the programmed target path). To quantify this, we calculated the ratio between the range of hand position and the range of adjusted target position. We averaged the ranges of the four cycles to get one value for each trial and then averaged across the 17 shapes and 6 subjects ($n=102$). The result was 0.82 (± 0.19 SD) for depth, compared to 0.98 (± 0.08 SD) and 1.04 (± 0.11 SD) for the horizontal and vertical dimensions, respectively. ANOVA with Scheffé's post hoc test showed that the value for the Y -dimension was significantly lower than for the X - and Z -dimensions, and also that the value for X was less than for Z ($F(2, 303) = 72.00, P < 0.001$).

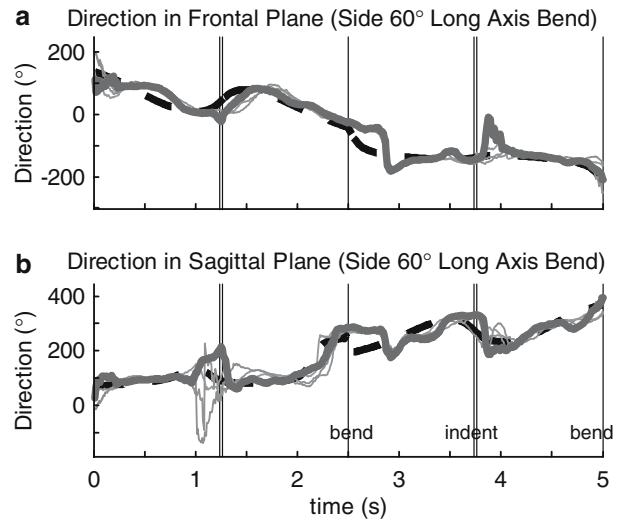


Fig. 5 Both indents and bends were disruptive to the tracking of target direction. Direction was calculated in two planes: the frontal plane (a) and the sagittal plane (b). The directions of the target and the hand are plotted over time for the same trial as in Figs. 3d and 4 (one subject, Side 60° Long Axis Bend). Target direction is shown with *thick, dashed black lines*. Vertical double lines indicate times when the target was at an indent of the shape and vertical single lines show the times when the target was at an abrupt bend. Hand direction from the first cycle is graphed as a *thick line*, and cycles 2–4 are graphed as *thin lines*

Tracking velocity in three dimensions

Velocity data for each dimension (for the same trial) are shown in the right column of Fig. 4. Target velocity was tracked very well, especially in the horizontal and vertical dimensions (Fig. 4b, f). Furthermore, the subject's velocity patterns were consistent across the cycles for each dimension, especially for cycles 2–4 (thin lines). However, the hand velocity lagged behind the target velocity, most obviously just after the target had a large change in velocity. For example, in the horizontal dimension, between 1,250 and 2,500 ms, the target velocity changed rapidly. The hand velocity followed this change with a slight lag.

In contrast to depth position where there was little similarity between traces representing the target and the hand (Fig. 4c), the hand's depth velocity clearly followed some of the large, smooth fluctuations in the target's depth velocity (Fig. 4d). This suggests that subjects may perform poorly for slow changes in target depth position, but may track the smooth, fast changes quite well. This would indicate that the tracking in depth is less responsive to the lowest frequencies in the target motion.

The influence of the target bends (the highest frequency in the target motion) was quite apparent in the hand velocity traces. For the bend at 2,500 ms (single vertical line in the middle of each graph), the target suddenly traveled in a direction that would not have been predicted from a smooth continuation of the target's trajectory prior to the bend. The subject responded with an overshoot in horizontal velocity (Fig. 4b) and responded substantially later in depth velocity (Fig. 4d). Thus, as might be expected, abrupt bends in the target trajectory could be quite disruptive to hand tracking.

Frequency response

The data presented in Fig. 4 suggest two interrelated conclusions. First, there seems to be a distinct corrective response following the bends, with a relatively long reaction time. Secondly, the overall lag seems to be longer for high- than for low-frequency components of the target motion. We quantified these phenomena using data from all subjects.

First, we focused on measuring the reaction time to a bend by doing cross-correlation analysis on the cycle 2–4 subsections ranging from 2,500 to 3,500 ms. Using a paired *t* test, we compared time lags for the Front and Side 60° Long shapes to the corresponding data from Front and Side Cassini shapes with no bends. We tested each of the six position and velocity parameters separately and found a significant difference (at $P < 0.01$) in each case. The results (in ms) for 60° Long shapes versus No Bend shapes were: –160 versus –70 for *X*-position, –179 versus –86 for *Y*-position, –180 versus –85 for *Z*-position, –177 versus –80 for *X*-velocity, –230 versus –114 for *Y*-velocity and –192 versus –91 for *Z*-velocity.

Thus the reaction to bends occurred after about –190 ms, compared to lags of about –90 ms for the comparable smooth sections. The analysis indicated the longest bend reaction time (–230 ms) when the cross-correlations were applied to data from the depth (*Y*) dimension.

We also used a standard frequency domain analysis to evaluate the reaction of the manual pursuit system to high- and low-frequency components of the complex target motion. We generated Bode plots to examine the gain and phase of the hand/target transfer function for each of the six positional and velocity parameters. For the *X*- and *Z*-dimensions at 0.6 and 0.2 Hz and for the *Y* (depth) dimension at 0.6 Hz, the analysis revealed gains near one and time lags near 100 ms. However, for the base frequency (0.2 Hz) in depth (*Y*), the analysis suggested low gains (around 0.7) and phase leads (around +380 ms). Since a 380 ms lead in only one dimension is implausible, we interpret this to suggest that tracking in depth of low-frequency components is very poor.

Limiting our quantification to the *X*- and *Z*-dimensions, we did a paired *t* test to compare time lags at the higher (0.6 Hz) and lower (0.2 Hz) frequencies for all subjects and all Cassini shapes. The average lags were –101 ms at 0.6 Hz and –88 ms at 0.2 Hz, and these values were significantly different from one another ($t = 5.57$, 278, $P < 0.001$). Thus both the cross-correlation and the transfer function analyses indicated that the hand tracking in the frontal plane was better (in terms of time lag) for the smooth, low-frequency portions of the complex trajectory.

Tracking direction in the frontal and sagittal planes

We found that the pattern of changes in hand direction matched the pattern of changes in target direction with a lag and some error (Fig. 5). The indents were not noticeably disruptive in position and velocity (see Fig. 4), but they produced many errors in direction (near the double lines in Fig. 5). During the indents, subjects often made small loops, with direction changing by 360°. Because the direction measure is circular, in the graphs in Fig. 5, a full rotation would appear as a smooth change in direction with a single, abrupt reversal at some point. An example of this is seen in the plot of sagittal plane direction (Fig. 5b) just prior to the midpoint of the first indent (approximately 1,050 ms) for the final two cycles (thin lines). Due to the point of view of the 3D graphs in Fig. 3d, it is difficult to determine whether the subject made a loop in the sagittal plane. However, we examined these cycles in detail and found that the subject did make a small loop on each of the final two cycles. Interestingly, a similar abrupt change in direction is not seen in the frontal plane direction because, while the hand made a change of 360° in direction from the sagittal view, it maintained correct motion in the frontal plane. Thus the 3D shape of the hand motion was a spiral.

In accord with the two-thirds power law (Lacquaniti et al. 1983) and the time course of the target motion, the hand slowed down during the tight curvature of the indent in the target path. Since direction was calculated using velocity values, if the X - or Y -component of velocity became zero, the directions in the fronto-parallel plane (Eq. 3) and the sagittal plane (Eq. 4) were undefined and the direction changed spuriously (as in the first cycle at the end of the second indent). Thus, the direction sometimes appears to change rapidly just because the subject slowed down.

In consonance with the results for velocity, the subject required a great deal of time to respond, in direction, to the bends (single vertical lines, Fig. 5). After the bend at 2,500 ms the target was traveling in a direction that was not predictable as a continuation of the previous motion. In both planes, the subject made a quick correction to align the hand motion with the direction of target motion. The correction was made in the frontal plane slightly sooner than that in the sagittal plane.

Distance and speed error during tracking

Average distance error for all subjects and Cassini shapes is shown in Fig. 6a for the first cycle (red line) and for the combination of all the other cycles (blue line). The vertical line hatching around each trace represents the 95% confidence interval. As in previous figures, the double vertical lines represent the time of the midpoint of indents and the single vertical lines show the times of all possible bends. (The long axis bends occurred at 2,500 and 5,000 ms, the oblique axis bends at 2,000 and 4,500 ms and the short axis bends at the midpoints of the indents.)

The pattern of distance errors was similar across the cycles. There was a large error at the beginning of the cycle (especially for the first cycle), then a reduction in that error beginning around 400 ms. Furthermore, after each of the indents and bends there was a small increase in distance error. Between 1,250 ms (first set of double lines) and 3,000 ms, the average distance error rose due to the indent and because of the increased occurrence of bends. The distance error decreased during the later half of the cycle, perhaps because subjects had a better estimate of the target shape after completing the first half. The error during the first cycle (red line) was considerably larger than during the other cycles (blue line) for the first 750 ms and appeared slightly larger than the other cycles until approximately 3,000 ms.

For all cycles, the unsigned speed error was large at the beginning of the cycle and after each possible bend (Fig. 6b). The signed speed error indicates that the subjects tended to slow down (negative error) after an indent or bend (Fig. 6c). Unsigned speed error decreased during times when the target motion was smooth (no bends or indents). During these times the signed speed error was positive, indicating that the subject used the smooth portions of the target motion to catch up.

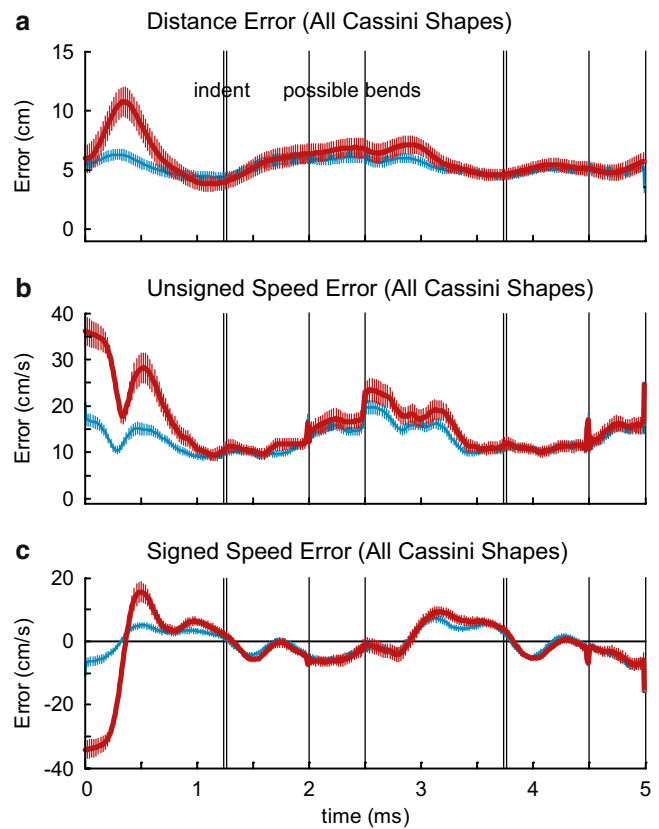


Fig. 6 Tracking improved during the first cycle. Average distance (a) and speed (b, c) errors across time for all Cassini shapes (all subjects). The error for the first cycle is graphed with *thick red lines* and cycles 2–4 are graphed with *thin blue lines*. The *vertical hatching around each line* represents 95% confidence intervals. The *vertical double lines* indicate times when the target reached the indents of the shape and the *single vertical lines* indicate the time when the target abruptly changed direction (all possible bends)

The first cycle was somewhat different from the others in that the unsigned speed error was much larger for the first 750 ms while the subject was responding to the onset of the target motion and catching up to the target (Fig. 6b). When the subjects did respond, they had to move faster to catch up to the target. They were moving slower than the target for the first 375 ms and then faster than the target from 375 to 1,350 ms (Fig. 6c). The unsigned error remained elevated compared to the other cycles until approximately 3,500 ms.

Distance, speed and direction error and lag across the cycles

In our measures of position, velocity and direction, it appears that the errors were largest in the first cycle. Thus, we tested for differences in the magnitude of errors and the time lags across the four cycles. The results of these analyses show that indeed there was more error and a greater lag during the first cycle (Fig. 7).

The first cycle had significantly more error than all the other cycles in over half the measures (open symbols in Fig. 7, see Table 2 for details). Furthermore, the trend was evident in all measures except for the frontal plane (FP) direction error (Fig. 7e). For some of the individual measures, not all subsequent cycles were significantly different from the first, but no data were contrary to the trend (see post hoc results in Table 2). Cycles 2–4 were always the same in every measure. Thus, these results indicate that much improvement was made during the first cycle and that little improvement was made thereafter.

In contrast to the other lag values (Fig. 7b, d, f), the depth position (*Y*) lead/lag showed a slight lead for the final three cycles. This is consistent with our frequency

domain analysis, showing that slow changes in depth position were tracked very poorly, perhaps resulting in spurious lead values. Subjects tended to track rapid changes in depth much better than slow changes in depth. As shown in Fig. 7d, velocity lags for all three dimensions showed steady-state lags around -100 ms for cycles 2–4. Thus for most parameters, lag was around -150 ms for the first cycle and -100 ms for cycles 2–4.

Instantaneous lag during each cycle

It was possible that in the first cycle, our error and lag measures were biased by the unavoidably large errors during the reaction time; this might largely account for the result shown in Fig. 7. Thus we created a measure of instantaneous lag (shown schematically in Fig. 8a), which allowed us to document fluctuations in position lag and to determine the time course of the improvement in performance within the first cycle.

The instantaneous lag for several shapes is presented in Fig. 8b–e (the same shapes as in Fig. 3). As in the previous figures, data from the first cycle are shown with a thick line and data from the other cycles are shown with thinner lines. Inevitably, due to the reaction time, the first part of the first cycle had more lag than the other cycles. However, the first cycle also had more lag than subsequent cycles until approximately 3,000 ms.

When we examined the average of all the Cassini shapes, we found that the first cycle had more lag than the other cycles for about 3 s of the 5 s (Fig. 8f). Due to the visual reaction time and the time needed to catch up to the target, for approximately the first 1,000 ms of the first cycle (red line), there was much more lag than for the other cycles (blue line). Around the time when the target slowed down for the indent (1,000–1,500 ms), the lags were similar across all four cycles, but from 1,690–3,150 ms, the lag in the first cycle was again significantly greater than the lag in the other cycles. Thus for the majority of the first 3 s of the first cycle, the subjects had more lag than in the other cycles. These results show that the main effect of increased lag during the first cycle is not simply due to the reaction time for starting the trial; it continues for about 3 s.

We wondered whether this value of 3 s represented an absolute time needed to engage predictive tracking or if, in contrast, the time depended on the amount of experience with specific features of the target shape. We therefore examined the averaged data for all 4-Plane shapes and found that the first cycle became as accurate as subsequent cycles after 2,310 ms (data not shown). This value of about 2.3 s did not differ depending on whether it was the subject's first, second or third experience with the 4-Plane shape; it corresponds to about half-way through the second (of four) semicircles, which were identical except for their spatial orientation.

We also modified our calculation of instantaneous lag to allow for a position lead and repeated the analysis for

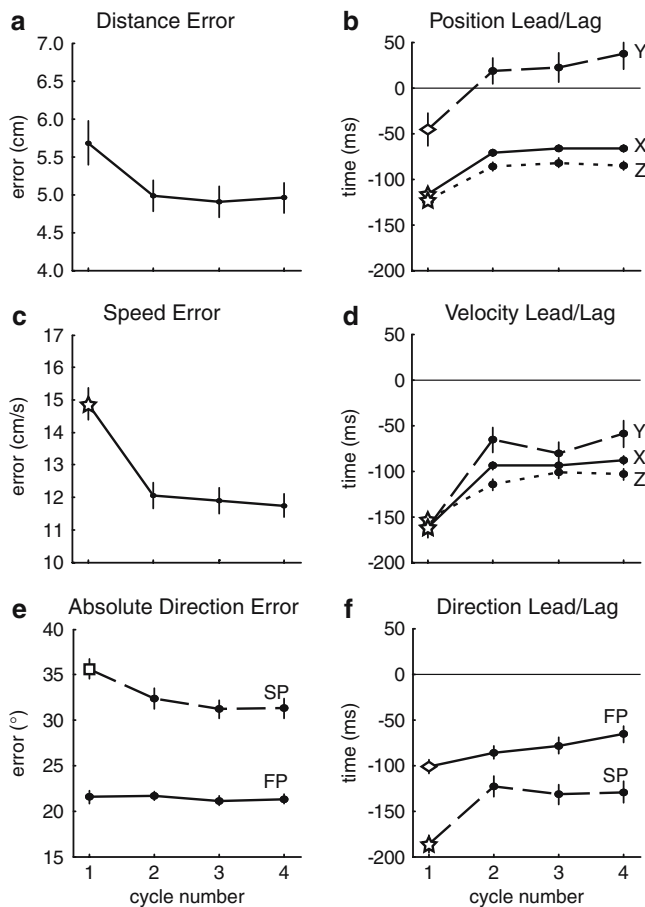


Fig. 7 Performance stabilized after the first cycle. The average error and lag values (all subjects and shapes) are plotted for each cycle (error bars represent ± 1 standard error of the grand mean for the six subjects). Errors for distance (a), speed (c) and direction (e) are shown in the left column. The lead/lag values for position (b), velocity (d) and direction (f) are shown in the right column. Negative values indicate that the subject was lagging behind the target. Stars were used as the symbol when the first cycle was significantly different from all other cycles. Diamonds were used when the first cycle was different from the fourth cycle and the square indicates that the first cycle was different from the third cycle. The second, third and fourth cycles were never significantly different from one another

Table 2 Main effects of cycle for each dependent variable (all shapes)

	<i>F</i>	<i>df</i>	<i>P</i>	Post hoc
Distance error	2.575	3, 404	0.054	
Abs. speed error	12.941	3, 404	<0.001	1 > 2, 3, 4
FP direction error	0.188	3, 404	0.905	
SP direction error	3.529	3, 404	0.015	1 > 3
<i>X</i> -position lag	44.323	3, 404	<0.001	1 > 2, 3, 4
<i>Y</i> -position lag	4.132	3, 325	0.007	1 > 4
<i>Z</i> -position lag	15.440	3, 403	<0.001	1 > 2, 3, 4
<i>X</i> -velocity lag	65.628	3, 403	<0.001	1 > 2, 3, 4
<i>Y</i> -velocity lag	11.865	3, 325	<0.001	1 > 2, 3, 4
<i>Z</i> -velocity lag	14.656	3, 403	<0.001	1 > 2, 3, 4
FP direction lag	3.298	3, 403	0.020	1 > 4
SP direction lag	6.954	3, 392	<0.001	1 > 2, 3, 4

Statistical data to illustrate that the first cycle (“1”) revealed significantly larger errors than the other cycles for most measures

all shapes. The results were very similar. We found that a slight lead (less than 40 ms) occurred only for the 4-Plane shapes and only near the end of each planar segment (at 3.0, 4.7 and 6.5 s; compare these times with Fig. 8c where no lead was allowed in the calculation).

Tracking error comparisons across the sections of the Cassini shapes

We examined the influence of the bends on performance by comparing the error and lag measures across comparable subcycles of the different shapes. If the bend caused a disruption in tracking, a subcycle after a bend would have more error than the comparable subcycle of a shape where there was no bend. The results of the analysis are detailed in Table 3 and drawn schematically in Fig. 9, where the entire Cassini shape is redrawn to represent each error measure. For example, the distance error is represented by the inside shape and the instantaneous lag measure is the outermost shape. Each set of shapes corresponds to a specific bend type: long (a), short (b) and oblique (c). The shaded areas indicate the sections of the shapes in which our hypothesis would predict more error if the bends were disruptive. The thick dashed lines indicate the sections where the error was significantly larger (see Table 3). In accord with our prediction, the highlighted sections for each bend type contain the most dashed lines.

Except in one case, the subcycles in the shape without bends did not have more error than the subcycles following bends (Table 3; frontal plane (FP) direction error in Section 3). For shapes that had a long axis bend (Fig. 9a), there was more speed and direction error and the lag was longer at the beginning of the shape (Section 1) and in the subcycle after the center of the shape (Section 4). For shapes with a short axis bend (Fig. 9b), there tended to be more error and longer lags in the sections just after the bends (Sections 2 and 5), but not in as many measures as for the other bend types. This may

be due to the fact that short axis bends occurred in conjunction with indents, which also caused errors in every shape type. The oblique bends caused the most error (Fig. 9c). Not only was the error larger just after the oblique bends (Sections 3 and 6) but also in other sections, suggesting that the irregularity of this shape may have degraded overall performance.

Tracking error comparisons across the three dimensions

From the position and velocity graphs in Fig. 4, the transfer function analysis and the summary data in Fig. 7, it appears that the subjects did not track as well in depth as they did in the horizontal and vertical dimensions. To further quantify the differences between tracking in each dimension, we used a measure of the strength of the relationship between the target and hand motion obtained when evaluating the time lag/lead for each dimension or plane.

As shown in Tables 4 and 5, for both position and velocity, during all the shapes, the relationship between target and hand motions was very high in the *X*- and *Z*-dimensions, with correlation coefficients ranging from 0.996 to 0.922. In contrast, correlations between the target and hand motions in the *Y*-dimension (depth) were significantly lower than for both the *X*- and *Z*-dimensions, ranging from 0.849 to 0.628. Furthermore, as mentioned under [Methods](#), compared with the *X*- and *Z*-dimensions, a much greater percentage of depth position and velocity data lacked a cross-correlation peak and thus were eliminated from this analysis (19% for depth position and 7% for depth velocity). Overall, these results indicate that the tracking in depth is not as good as tracking in the horizontal (*X*) and vertical (*Z*) dimensions for the Cassini shapes (Table 4) as well as the 4-Plane shapes (Table 5).

Discussion

We examined three main issues regarding subjects’ ability to track, with the hand, targets moving in 3D. First, we examined the improvement during the course of tracking multiple cycles around a given shape: tracking improved during the first 3 s of the first cycle and then stabilized for the last 2 s and across cycles 2–4. We also examined the errors resulting from tight path curvatures (indents) and abrupt changes in target trajectory (bends); we documented the marked fluctuations in tracking performance due to the fact that these features were interspersed with smooth planar segments (Figs. 4, 5, 6, 8, 9). Finally, we compared tracking in depth to tracking in the frontal plane. As expected, tracking in depth differed both qualitatively and quantitatively: subjects showed little modulation in depth position and inferior target/hand correlations for both position and velocity.

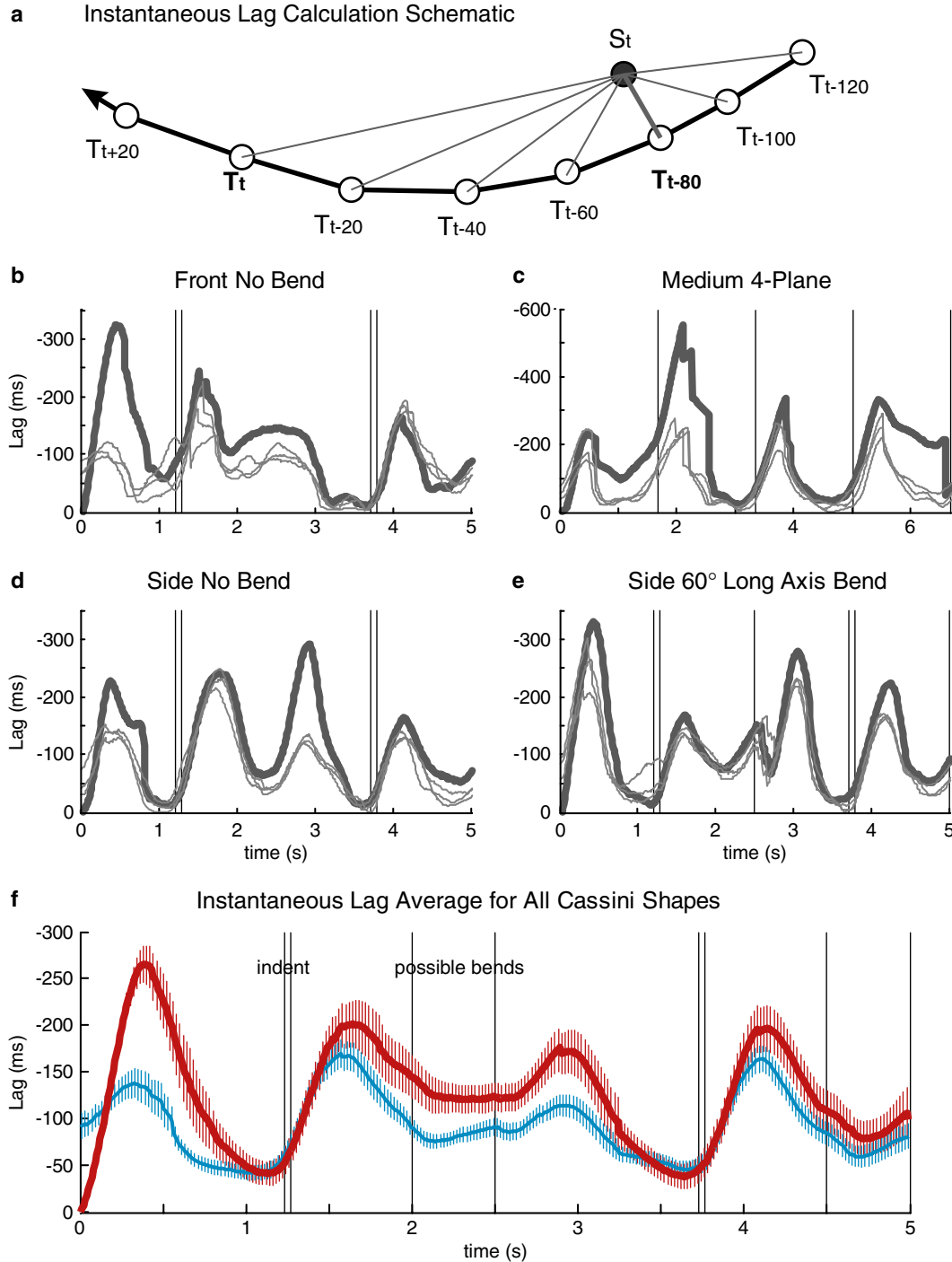


Fig. 8 For Cassini shapes, the time lag for hand tracking improved gradually during the first 3 s. The schematic in **a** shows how instantaneous lag was calculated. The current hand position is labeled H_t and the current target position is labeled T_t . Distance was calculated between the current hand position and the target at all positions (before and including the current position). The pair that produced the least error was found, and the time difference between the instantane-
ous lag and the current target position was computed. This time difference is defined as the instantaneous lag. For the example shown, the lag is -80 ms. The instantaneous lags for four shapes (one subject) are shown in this figure (b-e), with increasing negative (lag) values plotted upwards. The vertical double lines show the time when the target

was at the indents. The single vertical lines in **c** show the times when the target finished each semicircle and changed from horizontal to vertical planes. The lag for the first cycle is graphed with a thick line; the lags for cycles 2-4 are plotted with thin lines. We calculated the average instantaneous lag for all the Cassini shapes and compared the lag during the first cycle with the lag during the other three cycles (f). The first cycle is graphed with a thick red line, the average of all the other cycles with thin blue line (all subjects). The vertical hatching around each line represents the 95% confidence intervals. The vertical double lines show the times when the target was at the indent and the single vertical lines show the times of every possible bend

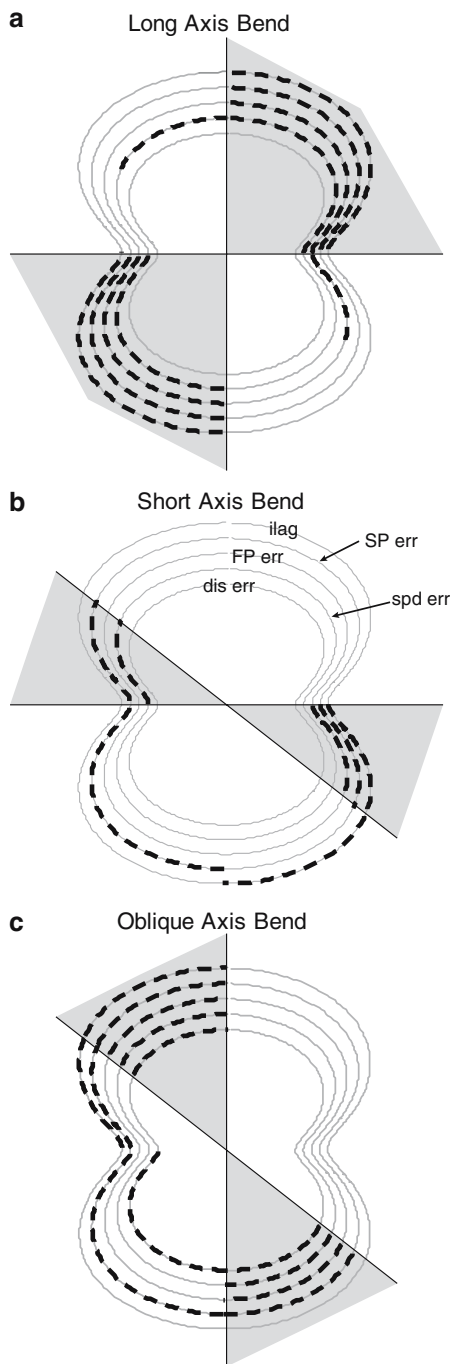


Fig. 9 Bends and shapes with oblique bends degraded tracking performance. For each bend [long axis (a), short axis (b) and oblique axis (c)], we examined the magnitude of the error or lag during each section (subcycle) of the Cassini shapes. A section is defined as the part of a shape between possible bends; every shape has six sections (see Fig. 1a). The *highlighted areas* in the schematics show the sections where we would expect more error and lag, if the bends were problematic. We compared the magnitude of the distance error (*dis err*) and speed error (*second line from inside, spd err*), frontal plane direction error (*FP err*), sagittal plane direction error (*second line from outside, SP err*) and instantaneous lag (*ilag*) during each section after each type of bend. The *thick dashed lines* indicate the sections where there was more error or a longer lag for each bend orientation (see Table 3 for details)

Anticipatory tracking and internal models

We were somewhat surprised to find that tracking improved so dramatically after 3 s (Figs. 6, 8). In previous studies, steady-state performance in hand or eye tracking was reached after one or two brief trials (Barnes and Marsden 2002; Barnes et al. 2000). It could be that improvements in the gain and lag of tracking simply require a certain amount of practice. However, in our study, we also noticed that for the Cassini shapes, 3 s corresponded to movement of the hand three-fifths of the distance around the shape. This put the hand beyond most of the bends and on its way into the second indent (see Fig. 8f). Since the shapes were basically symmetrical, it seems possible that at the three-fifth point, the tracking system may have begun to draw upon an estimate of the remaining target path. This idea was reinforced by finding that in tracking the even more regular 4-Plane shape, performance improved after 2.3 s, during the second of four equally sized semicircles.

Visual reaction time during hand tracking is known to be about 100 ms (Smith and Bowen 1980; Zelaznik et al. 1983; Prablanc and Martin 1992) and therefore, lags better than -100 ms suggest some form of anticipation. In addition to the dramatic overall improvement after 3 s, subjects exhibited fluctuations between 0 and -300 ms lag, depending on specific features of the target trajectory. The full-cycle velocity lags calculated using cross-correlation (Fig. 7d) represent a compromise across epochs of the tracking performance with various lags. Thus the improvement from -150 ms overall lag in the first cycle to a value of -100 ms in cycles 2–4 indicates that beyond the first 3 s, numerous tracking epochs had lags substantially less than -100 ms (see Fig. 8).

Shibata et al. (2005) have recently proposed a model of predictive smooth pursuit, which may also be applicable to anticipatory hand tracking. They simulated zero-lag oculomotor tracking of sine waves and velocity ramps using a recurrent neural network where weights were adjusted to learn future target velocities. Their algorithm was essentially similar to a Kalman filter and their implementation provided the tracking system with an “internal model” of target dynamics. Whether or not their simulation can learn more complex target trajectories remains an open question.

Other models of manual and smooth pursuit tracking do not incorporate the learning of target dynamics and instead, inputs related to current target velocity are used to derive an error signal to drive hand or eye acceleration (Engel and Soechting 2000; Churchland and Lisberger 2001). These tracking models do not explain the relatively short tracking lags in the present study. Thus we propose that the short lags in our study may be due to the use of an internal target trajectory as the target for the tracking response. This “internal model” may simply represent a smooth continuation of a two-thirds power trajectory or could possibly incorporate higher order features such as the fact that the path is symmetrical and

Table 3 ANOVA's comparing bend types (Cassini shapes only)

	<i>F</i> (3, 332)	<i>P</i>	Post hoc
Section 1			
Distance error	0.857	0.464	
Speed error	20.091	< 0.001	Long > all
FP direction error	19.708	< 0.001	Long > all
SP direction error	19.246	< 0.001	Long > all
Instantaneous lag	3.652	0.013	Long > oblique
Section 2			
Distance error	1.397	0.244	
Speed error	2.471	0.062	
FP direction error	13.230	< 0.001	Long, short > no, oblique
SP direction error	18.634	< 0.001	Short > all
Instantaneous lag	4.465	0.004	Short > oblique
Section 3			
Distance error	1.968	0.002	Oblique > no, long
Speed error	8.779	< 0.001	Oblique > long, short
FP direction error	67.631	< 0.001	Oblique > all; no > short
SP direction error	13.714	< 0.001	Oblique > all
Instantaneous lag	4.501	0.004	Short > oblique
Section 4			
Distance error	4.963	0.002	Oblique > short
Speed error	33.113	< 0.001	Long > all
FP direction error	10.291	< 0.001	Long > no, oblique
SP direction error	15.863	< 0.001	Long > oblique > no; short > no
Instantaneous lag	3.938	0.009	Long , oblique > no
Section 5			
Distance error	2.605	0.052	
Speed error	7.892	< 0.001	Short > no, long
FP direction error	1.269	0.285	
SP direction error	26.851	< 0.001	Short > all; oblique > long
Instantaneous lag	5.808	< 0.001	Oblique > no, short
Section 6			
Distance error	3.949	0.009	Oblique > no
Speed error	22.291	< 0.001	Oblique > long > no, short
FP direction error	51.770	< 0.001	Oblique > all
SP direction error	19.511	< 0.001	Oblique > all
Instantaneous lag	6.217	< 0.001	Oblique > long, no

Statistical analysis of errors for position, speed, direction in frontal plane (FP) and sagittal plane (SP) and lag for the six sections of the Cassini shape between the bends (see Fig. 1a). The hypothesis that the section of the cycle after a bend would have more error than the corresponding section where there was no bend was tested. The fourth column shows the results of a post hoc analysis. In each case, the type of shape predicted to have more error is listed in boldface type

closed (i.e., that the target will return to its starting location).

Thus, the improvement in hand tracking after 3 s may be somewhat analogous to the gradual improvement in reaching movements as subjects form an "internal model" of the physical properties of a novel environment (e.g., Krakauer et al. 1999). The concept of

the internal model has been very valuable to the field of motor control (Wolpert et al. 1995; Desmurget and Grafton 2000). The internal model is a mapping between the desired movement and the motor commands necessary to produce that movement. The proper mapping depends critically upon the physical properties of the object to be moved, and the brain is thought to store

Table 4 Strength of hand–target correlations for Cassini shapes (all cycles)

	Shifted <i>r</i>	Shifted <i>Z</i> -score	<i>F</i> ^a	<i>df</i>	<i>P</i>
<i>X</i> -position	0.993 ± 0.004	0.393 ± 0.041	286.004	2, 935	< 0.001
<i>Y</i> -position ^b	0.849 ± 0.156	−0.979 ± 1.477			
<i>Z</i> -position	0.992 ± 0.010	0.382 ± 0.093			
<i>X</i> -velocity	0.937 ± 0.034	0.579 ± 0.190	784.402	2, 984	< 0.001
<i>Y</i> -velocity ^b	0.628 ± 0.190	−1.143 ± 1.057			
<i>Z</i> -velocity	0.922 ± 0.041	0.493 ± 0.227			

Correlation values between target (Cassini shape) and hand for position and velocity are given. Correlation values for the *Y*-dimension (depth) were significantly lower than for the other dimensions

^aANOVAs were performed on *Z*-scores

^bDifferent than others

Table 5 Strength of hand–target correlations for 4-Plane shapes (all cycles)

	Shifted r	Shifted Z -score	F^a	df	P
X -position	0.996 ± 0.002	0.430 ± 0.018	70.657	2, 202	< 0.001
Y -position ^b	0.825 ± 0.171	-0.961 ± 1.391			
Z -position	0.995 ± 0.005	0.423 ± 0.039			
X -velocity	0.943 ± 0.030	0.439 ± 0.196	62.769	2, 203	< 0.001
Y -velocity ^b	0.739 ± 0.208	-0.918 ± 1.375			
Z -velocity	0.936 ± 0.040	0.389 ± 0.262			

Correlation values between target (4-Plane shape) and hand for position and velocity are given. Correlation values for the Z -dimension (depth) were significantly lower than for the other dimensions

^aANOVAs were performed on Z -scores

^bDifferent than others

anticipated properties and use experienced properties to update this stored representation. Since hand tracking is essentially a process of interacting with a moving target, learning to anticipate features of the trajectory may be similar to internal model learning. An internal representation of the anticipated target trajectory would allow the system to predict and evaluate the expected consequence (i.e., the desired error reduction) of each incremental tracking movement.

Frequency response and pulsatile corrections

In the present set of experiments, target trajectories were designed to be unfamiliar but symmetric and therefore relatively easy to remember for reproduction (in the memory condition reported in Flanders et al. 2005). The shapes were also broken into planar segments in accord with the hypothesis that it is easy to move the hand in a plane but difficult to change planes (Soechting et al. 1986; Soechting and Terzuolo 1987a, b). For the tracking trials, we also chose to program the target to move in good approximation to the two-thirds power law (Lacquaniti et al. 1983; see Flanders et al. 2005), and this resulted in trajectories with a range of speeds and curvatures, interspersed between sharp bends. As expected, subjects tracked better during the smooth segments (Viviani et al. 1987).

Some of the fluctuations in tracking performance within each cycle may essentially represent the “frequency response” of the tracking system, in that certain accelerations are beyond the capabilities of the system. As mentioned in Introduction, Kettner et al. (1996) evaluated the frequency response of 2D smooth pursuit eye movements and found a progressive increase in lag for higher frequency target motions. In our study, the abrupt bends may be regarded as high frequencies in the target trajectory. We found abrupt responses with prolonged reaction times (about 190 ms) following bends. We also found that tracking at the base frequency (0.2 Hz) had significantly less lag than tracking at a higher frequency (0.6 Hz).

Tracking in depth

Manual tracking was better in the horizontal and vertical dimensions than in the depth dimension. The positional and directional errors were greater in depth, and the target/hand correlations for both position and velocity were significantly worse in depth. We also reported a meager amplitude gain for depth position, a good response to relatively fast but smooth changes in depth velocity and a delayed response to abrupt changes in depth velocity (Fig. 4c, d). The overall time lag for tracking depth velocity was similar to that for the horizontal and vertical dimensions (Fig. 7d), but other aspects of the depth response seemed quite different.

Although it was not clear exactly how frontal plane and depth tracking would differ, differences were expected, due to the very different motion cues and the differential involvement of conjugate and vergence eye movements, for tracking in the frontal plane and tracking in depth, respectively. As mentioned in Introduction, oculomotor tracking is much better in the frontal plane than in depth (Gielen et al. 2004). Furthermore, the vergence eye movements are more variable than smooth pursuit, and the vergence system has complex interactions with the conjugate eye movement systems (Chaturvedi and Van Gisbergen 1998; Semmlow et al. 1998). Assuming that the eye followed the target in our task, these complications in oculomotor control were expected to have a counterpart in hand–eye coordination and manual control.

However, in another sense, the poor performance in depth seems somewhat contrary to the well-known ability of humans to estimate time to contact for catching. Stereopsis and time to contact cues (i.e., the rate of retinal expansion) have been shown to strongly contribute to accurate catching performance (Mazyn et al. 2004; Savelsbergh et al. 1992, 1993). Recently, however, Zago et al. (2004) have pointed out that pure visual cues are not sufficient to explain subjects’ behavior in a manual interception task. Instead, subjects’ interception behavior relied heavily upon an internal model of a real ball falling with acceleration due to gravity or, alternatively, a video image of a ball moving downward with constant speed.

Studies of manual tracking in depth are hampered by the fact that real targets may come in physical contact with the hand, but virtual targets may lack some of the natural depth cues. In the present study, the virtual target provided strong size and disparity cues, but lacked other cues such as vergence and accommodation. Size cues provide good motion-in-depth signals to both the perceptual and the manual tracking systems (Lopez-Moliner et al. 2003), but other motion-in-depth cues may be used differently depending on the (perceptual or motor) goal of the task (e.g., Harris and Drga 2005). In spite of the limitations, however, one advantage to a virtual target display is that it can be programmed to present trajectories that systematically vary particular parameters and cause controlled gaps or perturbations

in the target presentation. Future work can combine a more systematic analysis of trajectory parameters and perturbations with modeling/simulation studies (such as that of Shibata et al. 2005).

Acknowledgements This work was supported by NIH grant R01 NS027484. We thank Professor John F. Soechting for helpful discussions.

References

- Adamovich SV, Berkinblit MB, Fookson O, Poizner H (1998) Pointing in 3D space to remembered targets. I. Kinesthetic versus visual target presentation. *J Neurophysiol* 79:2833–2846
- Admiraal MA, Keijsers NLW, Gielen CCAM (2003) Interaction between gaze and pointing toward remembered visual targets. *J Neurophysiol* 90:2136–2148
- Barnes GR, Marsden JF (2002) Anticipatory control of hand and eye movements in humans during oculo-manual tracking. *J Physiol* 539:317–330
- Barnes GR, Barnes DM, Chakraborti SR (2000) Ocular pursuit responses to repeated, single-cycle sinusoids reveal behavior compatible with predictive pursuit. *J Neurophysiol* 84:2340–2355
- Bock O (1986) Contribution of retinal versus extraretinal signals towards visual localization in goal-directed movements. *Exp Brain Res* 64:476–482
- Chaturvedi V, Van Gisbergen JA (1998) Shared target selection for combined version-vergence eye movements. *J Neurophysiol* 80:849–862
- Churchland MM, Lisberger SG (2001) Experimental and computational analysis of monkey smooth pursuit eye movements. *J Neurophysiol* 86:741–759
- Dallos PJ, Jones RW (1963) Learning behavior of the eye fixation control system. *IEEE Trans Automat Control* 8:218–227
- Desmurget M, Grafton S (2000) Forward modeling allows feedback control for fast reaching movements. *Trends Cogn Sci* 4:423–431
- Engel KC, Soechting JF (2000) Manual tracking in two dimensions. *J Neurophysiol* 83:3483–3496
- Flanders M, Mrotok LA, Gielen CCAM (2005) Planning and drawing complex shapes. *Exp Brain Res* (DOI 10.1007/s00221-005-0252-2)
- Gielen CCAM, Gabel SF, Duysens J (2004) Retinal slip during active head motion and stimulus motion. *Exp Brain Res* 155:211–219
- Harris JM, Drga VF (2005) Using visual direction in three-dimensional motion perception. *Nat Neurosci* 8:229–233
- Henriques DYP, Klier EM, Smith MA, Lowy D, Crawford JD (1998) Gaze-centered remapping of remembered visual space in an open-loop pointing task. *J Neurosci* 18:1583–1594
- Kettner RE, Leung HC, Peterson BW (1996) Predictive smooth pursuit of complex two-dimensional trajectories in monkey: component interactions. *Exp Brain Res* 108:221–235
- Krakauer JW, Ghilardi M-F, Ghez C (1999) Independent learning of internal models for kinematic and dynamic control of reaching. *Nat Neurosci* 2:1026–1031
- Lacquaniti F, Terzuolo C, Viviani P (1983) The law relating the kinematic and figural aspects of drawing movements. *Acta Psychol Amst* 54:115–130
- Lopez-Moliner J, Smeets JBJ, Brenner E (2003) Similar effects of a motion-in-depth illusion on tracking and perceptual judgements. *Exp Brain Res* 151:553–556
- Mazyn LI, Lenoir M, Montagne G, Savelsbergh GJ (2004) The contribution of stereo vision to one-handed catching. *Exp Brain Res* 157:383–390
- Medendorp WP, Crawford JD (2002) Visuospatial updating of reaching targets in near and far space. *Neuroreport* 13:633–636
- Poulton EC (1974) Tracking skill and manual control. Academic, London
- Prablanc C, Martin O (1992) Automatic control during hand reaching at undetected two-dimensional target displacements. *J Neurophysiol* 67:455–469
- Roitman AV, Massaquoi SG, Takahashi K, Ebner TJ (2004) Kinematic analysis of manual tracking in monkeys: characterization of movement intermittencies during a circular tracking task. *J Neurophysiol* 91:901–911
- Savelsbergh GJ, Whiting HT, Burden AM, Bartlett RM (1992) The role of predictive visual temporal information in the coordination of muscle activity in catching. *Exp Brain Res* 89:223–228
- Savelsbergh GJ, Whiting HT, Pijpers JR, van Santvoord AA (1993) The visual guidance of catching. *Exp Brain Res* 93:148–156
- Semmlow JL, Yuan W, Alvarez TL (1998) Evidence for separate control of slow version and vergence eye movements: support for Hering's Law. *Vision Res* 38:1145–1152
- Shibata T, Tabata H, Schaal S, Kawato M (2005) A model of smooth pursuit based on learning target dynamics. *Neural Netw* 18:213–224
- Smith WM, Bowen KF (1980) The effects of delayed and displaced visual feedback on motor control. *J Mot Behav* 12:91–101
- Soechting JF, Flanders M (1989a) Sensorimotor representations for pointing to targets in three-dimensional space. *J Neurophysiol* 62:582–594
- Soechting JF, Flanders M (1989b) Errors in pointing are due to approximations in sensorimotor transformations. *J Neurophysiol* 62:595–608
- Soechting JF, Terzuolo CA (1986) An algorithm for the generation of curvilinear wrist motion in an arbitrary plane in three-dimensional space. *Neuroscience* 19:1393–1405
- Soechting JF, Terzuolo CA (1987a) Organization of arm movements. Motion is segmented. *Neuroscience* 23:39–51
- Soechting JF, Terzuolo CA (1987b) Organization of arm movements in three-dimensional space. Wrist motion is piecewise planar. *Neuroscience* 23:53–61
- Soechting JF, Lacquaniti F, Terzuolo CA (1986) Coordination of arm movements in three-dimensional space. Sensorimotor mapping during drawing movement. *Neuroscience* 17:295–311
- Soechting JF, Engel KC, Flanders M (2001) The Duncker illusion and eye-hand coordination. *J Neurophysiol* 85:843–854
- Viviani P, Campadelli P, Mounoud P (1987) Visuo-manual pursuit tracking of human two-dimensional movements. *J Exp Psychol Hum Percept Perform* 13:62–78
- Wolpert DM, Ghahramani Z, Jordan MI (1995) An internal model for sensorimotor integration. *Science* 269:1880–1882
- Yasui S, Young LR (1975) Perceived visual motion as an effective stimulus to pursuit eye movement system. *Science* 190:906–908
- Zago M, Bosco G, Maffei V, Iosa M, Ivanenko YP, Lacquaniti F (2004) Internal models of target motion: expected dynamics overrides measured kinematics in timing manual interceptions. *J Neurophysiol* 91:1620–1634
- Zelaznik HZ, Hawkins B, Kisselburgh L (1983) Rapid visual feedback processing in single-aiming movements. *J Mot Behav* 15:217–236